

LETTER TO THE EDITOR

## A candidate circumbinary Keplerian disk in G35.20–0.74 N: A study with ALMA

Á. Sánchez-Monge<sup>1</sup>, R. Cesaroni<sup>1</sup>, M. T. Beltrán<sup>1</sup>, M. S. N. Kumar<sup>2</sup>, T. Stanke<sup>3</sup>, H. Zinnecker<sup>4</sup>, S. Etoka<sup>5,6</sup>, D. Galli<sup>1</sup>,  
C. A. Hummel<sup>3</sup>, L. Moscadelli<sup>1</sup>, T. Preibisch<sup>7</sup>, T. Ratzka<sup>7</sup>, F. F. S. van der Tak<sup>8,9</sup>, S. Vig<sup>10</sup>,  
C. M. Walmsley<sup>1,11</sup>, and K.-S. Wang<sup>12</sup>

<sup>1</sup> INAF, Osservatorio Astrofisico di Arcetri, Largo E. Fermi 5, 50125 Firenze, Italy  
e-mail: asanchez@arcetri.astro.it

<sup>2</sup> Centro de Astrofísica da Universidade do Porto, Rua das Estrelas, 4150-762 Porto, Portugal

<sup>3</sup> ESO, Karl-Schwarzschild-Strasse 2, 85748 Garching bei München, Germany

<sup>4</sup> SOFIA Science Center, NASA Ames Research Center, Mailstop 232-12, Moffett Field, CA 94035, USA

<sup>5</sup> Jodrell Bank Centre for Astrophysics, School of Physics and Astronomy, University of Manchester, Manchester M13 9PL, UK

<sup>6</sup> Hamburger Sternwarte, Gojenbergsweg 112, 21029 Hamburg, Germany

<sup>7</sup> Universitäts-Sternwarte München, Ludwig-Maximilians-Universität, Scheinerstrasse 1, 81679 München, Germany

<sup>8</sup> SRON Netherlands Institute for Space Research, PO Box 800, 9700 AV Groningen, The Netherlands

<sup>9</sup> Kapteyn Astronomical Institute, University of Groningen, 9700 AV Groningen, The Netherlands

<sup>10</sup> Department of Earth and Space Science, Indian Institute of Space Science and Technology, Thiruvananthapuram, 695 547 Kerala, India

<sup>11</sup> Dublin Institute for Advanced Studies (DIAS), 31 Fitzwilliam Place, Dublin 2, Ireland

<sup>12</sup> Leiden Observatory, Leiden University, PO Box 9513, 2300 RA Leiden, The Netherlands

Received 19 January 2013 / Accepted 15 March 2013

### ABSTRACT

We report on ALMA observations of continuum and molecular line emission with  $0''.4$  resolution towards the high-mass star-forming region G35.20–0.74 N. Two dense cores are detected in typical hot-core tracers (e.g.,  $\text{CH}_3\text{CN}$ ) that reveal velocity gradients. In one of these cores, the velocity field can be fitted with an almost edge-on Keplerian disk rotating about a central mass of  $\sim 18 M_\odot$ . This finding is consistent with the results of a recent study of the CO first overtone bandhead emission at  $2.3 \mu\text{m}$  towards G35.20–0.74 N. The disk radius and mass are  $\geq 2500$  au and  $\sim 3 M_\odot$ . To reconcile the observed bolometric luminosity ( $\sim 3 \times 10^4 L_\odot$ ) with the estimated stellar mass of  $18 M_\odot$ , we propose that the latter is the total mass of a *binary* system.

**Key words.** stars: formation – ISM: individual objects: G35.20-0.74N – ISM: jets and outflows

## 1. Introduction

While different scenarios have been proposed to explain the formation of high-mass (i.e. OB-type) stars (monolithic collapse in a turbulence-dominated core – Krumholz et al. 2009; competitive accretion driven by a stellar cluster – Bonnell & Bate 2006; Bondi-Hoyle accretion – Keto 2007; see also the review by Zinnecker & Yorke 2007), all of them predict the formation of circumstellar disks. It is thus surprising that only a handful of disk candidates have been observed in association with massive (proto)stars. As a matter of fact, despite many observational efforts, convincing evidence of disks has been found only around early B-type (proto)stars, while circumstellar disks around O-type stars remain elusive (Wang et al. 2012; Cesaroni et al. 2007 and references therein). Moreover, a detailed investigation of the disk properties, comparable to those performed in disks around low-mass stars (e.g. Dutrey et al. 2007) is still missing due to the large distances of OB-type (proto)stars and the limited angular resolution at (sub)millimeter wavelengths. With the advent of the Atacama Large Millimeter Array (ALMA), the situation is bound to improve dramatically, since resolutions  $\ll 1''$  will be easily obtained.

With this in mind, we performed ALMA Cycle 0 observations of two IR sources containing B-type (proto)stars. These were chosen on the basis of their luminosities (on the order of  $10^4 L_\odot$ ), presence of bipolar nebulosities/outflows, detection of broad line wings in typical jet/outflow tracers (SiO), and strong emission in hot molecular core (HMC) tracers (such as methyl cyanide,  $\text{CH}_3\text{CN}$ ). Here we present the most important results obtained for one of the two sources, G35.20–0.74 N.

G35.20–0.74 N is a well known star-forming region located at a distance of  $2.19^{+0.24}_{-0.20}$  kpc (Zhang et al. 2009), with a luminosity of  $\sim 3 \times 10^4 L_\odot$ <sup>1</sup>. The region is characterized by a butterfly shaped reflection nebula oriented NE–SW (see Fig. 1), as well as a bipolar molecular outflow in the same direction, observed in  $^{12}\text{CO}$  by Dent et al. (1985a), Gibb et al. (2003; hereafter GHLW), Birks et al. (2006; hereafter BFG), and López-Sepulcre et al. (2009). The  $^{12}\text{CO}(1-0)$  line emission also appears to trace a N–S collimated flow (see BFG), coinciding with a thermal radio jet (Heaton & Little 1988; GHLW) seen also at IR wavelengths (Dent et al. 1985b; Walther et al. 1990; Fuller et al. 2001; De Buizer 2006; Zhang et al. 2013). It has been proposed that

<sup>1</sup> Estimate taken from the rms database, available at [http://www.ast.leeds.ac.uk/cgi-bin/RMS/RMS\\_DATABASE.cgi](http://www.ast.leeds.ac.uk/cgi-bin/RMS/RMS_DATABASE.cgi)

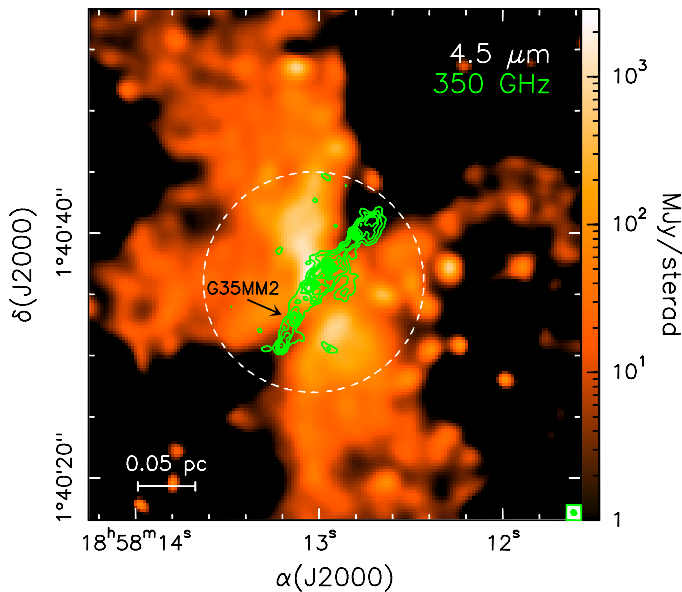


**Fig. 1.** Large-scale image of the  $4.5\ \mu\text{m}$  emission towards the star-forming region G35.20–0.74N overlaid with a contour map of the 350 GHz continuum emission obtained with ALMA. The IR image has been obtained by applying HiRes deconvolution (Velusamy et al. 2008) to the *Spitzer*/IRAC data. The sub-mm map has been corrected for primary beam attenuation. The contours range from 9 to 203 mJy/beam in steps of 10.8 mJy/beam. The dashed circle denotes the primary beam of the ALMA 12-m antennas. The ellipse in the bottom right is the ALMA synthesized beam.

the poorly collimated NE–SW outflow and the N–S jet could be manifestations of the same bipolar flow undergoing precession (Little et al. 1998). However, evidence for multiple outflows in this region is provided by SiO,  $\text{H}^{13}\text{CO}^+$ ,  $\text{H}^{13}\text{CN}$ , and  $\text{H}_2$  line observations (GHLW; Lee et al. 2012).

A molecular clump elongated perpendicular to the NE–SW outflow has been mapped in dense gas tracers ( $\text{NH}_3$ , CS), whose emission exhibits a velocity gradient from NW to SE (Little et al. 1985; Brebner et al. 1987). This was first interpreted as a large ( $\sim 1'$  or 0.6 pc) disk/toroid rotating about the NE–SW outflow axis, but on the basis of their  $\text{H}^{13}\text{CO}^+$  and  $\text{H}^{13}\text{CN}$  observations, GHLW propose that this is actually a fragmented rotating envelope containing multiple young stellar objects (YSOs). Indeed, GHLW identify a core at the center of the outflow and another core, named G35MM2, offset to the SE.

## 2. Observations and results

G35.20–0.74N was observed with ALMA Cycle 0 at 350 GHz in May and June 2012 with baselines in the range 36–400 m, providing sensitivity to structures  $\leq 2''$ . The digital correlator was configured in four spectral windows (with dual polarization) of 1875 MHz and 3840 channels each (covering the ranges 334.85–338.85 GHz and 346.85–350.85 GHz), providing a resolution of  $\sim 0.4\ \text{km s}^{-1}$ . Flux, gain, and bandpass calibrations were obtained through observations of Neptune and J1751+096. The data were calibrated and imaged using CASA. A continuum map was obtained from line-free channels and subtracted from the data. The synthesized beam is  $0'.51 \times 0'.46$ , PA =  $48^\circ$ . The rms noise is  $\sim 6\ \text{mJy beam}^{-1}$  for individual line channels, while in the continuum image, it is  $\sim 1.8\ \text{mJy beam}^{-1}$ , implying a S/N of only  $\sim 100$ . The latter indicates a reduced dynamic range.

In Fig. 1, we present the map of the 350 GHz continuum emission overlaid on an enhanced resolution *Spitzer*/IRAC

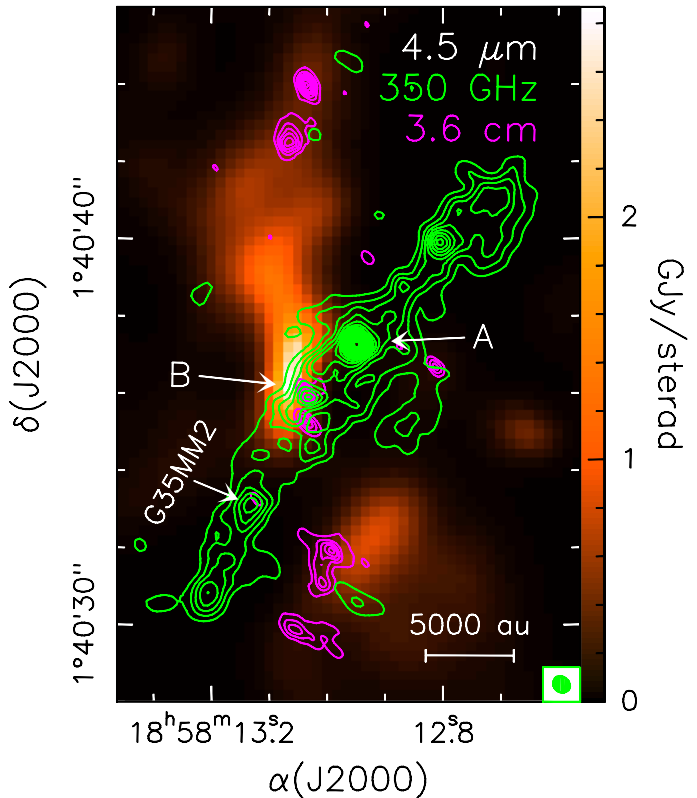


**Fig. 2.** Same as Fig. 1, with the 3.6 cm continuum map by GHLW overlaid (magenta contours). Unlike Fig. 1, the  $4.5\ \mu\text{m}$  image is displayed using linear scaling to emphasize the brightest structures outlining the N–S jet. Cores A, B, and G35MM2 are indicated by the arrows.

image at  $4.5\ \mu\text{m}$  extracted from the GLIMPSE survey (Benjamin et al. 2003). The sub-mm continuum emission is clearly tracing an elongated structure across the waist of the butterfly-shaped nebula. In all likelihood, we are detecting the densest part of the flattened molecular structure observed on a larger scale by Little et al. (1985), Brebner et al. (1987), and GHLW.

Along the elongated structure a chain of at least five cores is seen (Fig. 2), lending support to GHLW's idea that one is dealing with a fragmented structure instead of the smooth disk or toroid hypothesized by Little et al. (1985). We stress that the angular resolution of our maps ( $\sim 7$  times better than previous (sub)millimeter observations) reveals that the YSOs powering the outflow(s) lie inside cores A and/or B (see Fig. 2), because these two are the only cores located close to the geometrical center of the bipolar nebula. In particular, core B lies along the N–S jet traced by the IR and radio emission, and coincides with one of the free-free sources detected by GHLW. The hypothesis by BFG that core G35MM2 could be driving the NE–SW outflow is not convincing, because this core is off-center, lying right at the border of the waist outlined by the IR emission.

Methyl cyanide emission (as well as other typical HMC tracers) is clearly detected only towards cores A and B, and marginally towards G35MM2. Emission by vibrationally excited lines of  $\text{CH}_3\text{CN}$  also indicates that cores A and B could be hosting massive stars. Core B also coincides with a compact free-free continuum source detected by GHLW at 6 cm and 3.6 cm, and by Codella et al. (2010) at 1.3 cm. This emission could be part of the N–S thermal radio jet or might be coming from an HII region ionized by an embedded early-type star. We discuss this possibility in Sect. 4. Faint radio emission at a  $5.6\sigma$  level is also

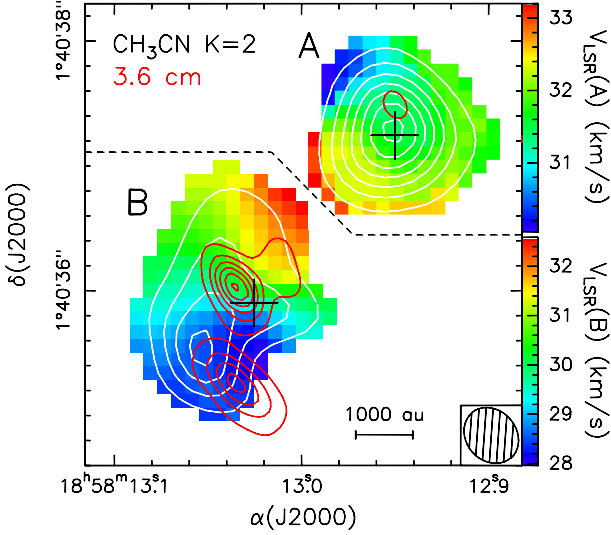


**Fig. 3.** Overlay of the average emission in the  $\text{CH}_3\text{CN}(19-18) K = 2$  line (white contours) and 3.6 cm free-free continuum emission (red contours; from GHLW) on a map of the first moment (i.e. velocity) of the same  $\text{CH}_3\text{CN}$  line. The velocity intervals used to calculate the mean emission and first moment are  $25.9-38.0 \text{ km s}^{-1}$  for core A and  $25.9-33.0 \text{ km s}^{-1}$  for core B. The dashed line is intended to stress that different color scales are used for the two cores to emphasize the velocity gradients. The white contour levels range from 80 to 656 mJy/beam in steps of 96 mJy/beam. The crosses mark the positions of the 350 GHz continuum peaks. The ellipse in the bottom right indicates the synthesized beam.

detected towards core A, consistent with the presence of one or more embedded star.

We now investigate the gas velocity field in the two cores by computing the first moment of a  $\text{CH}_3\text{CN}$  line, a dense gas tracer. Figure 3 plots the result for the  $\text{CH}_3\text{CN}(19-18) K = 2$  line, with the line emission overlaid that is averaged over the same velocity interval used to calculate the first moment. The mean velocity of core B ( $\sim 30 \text{ km s}^{-1}$ ) differs by  $\sim 2 \text{ km s}^{-1}$  from that of core A ( $\sim 32 \text{ km s}^{-1}$ ), which also differs by a similar amount from what is obtained ( $\sim 34 \text{ km s}^{-1}$ ) with lower angular resolution observations of other tracers (see e.g. GHLW). Discrepancies of this type are often found in high-mass star-forming regions (see, e.g., the case of AFGL5142 – Estalella et al. 1993; Zhang et al. 2007) and are very likely related to the fragmentation process in molecular clumps. The interesting result is that both cores present velocity gradients, which may be due to expansion or rotation of the gas. The sense of the gradient in core B is the opposite of what is measured on larger scales (see Fig. 5 of Little et al. 1985, and Figs. 8 and 9 of GHLW). However, the velocity range traced by the extended emission ( $30-41 \text{ km s}^{-1}$ ) differs significantly from the range sampled by the  $\text{CH}_3\text{CN}$  lines ( $\sim 26-38 \text{ km s}^{-1}$ ), suggesting that we are observing cores whose velocity field is not tightly related to that of the largest, fragmenting structure where they are embedded. In the following, we address this question for core B, which is better resolved and associated with the N–S jet/outflow.

### 3. The nature of core B: A Keplerian rotating disk?

An elongated structure with a velocity gradient along its major axis, such as the one observed in core B, can be interpreted as either a collimated bipolar outflow or a rotating ring/disk seen

close to edge on. We thus first investigate the possibility that we are observing the root of a large-scale bipolar outflow.

At first glance, both the orientation (see Fig. 2) and sign of the velocity gradient seen in Fig. 3 appear consistent with those of the N–S jet imaged by BFG (see the red-shifted emission at  $40 \text{ km s}^{-1}$  in their Fig. 3). However, the CO emission in the northern jet lobe is also detected by BFG at  $28 \text{ km s}^{-1}$  (see their Fig. 3), namely at blue-shifted velocities. Moreover, the direction of the  $\text{CH}_3\text{CN}$  velocity gradient has a negative position angle, whereas the jet is slightly inclined to the east. Such a difference could be explained if the jet is precessing (as suggested by BFG) and lies close to the plane of the sky, because the jet direction would change from the small to the large scale. We believe that this explanation is not satisfactory, because the orientation of the  $\text{CH}_3\text{CN}$  velocity gradient differs from that of the radio jet *on the same scale*. This can be seen in Fig. 3, where the two free-free emission sources are aligned N–S, whereas the velocity gradient (and the core major axis) are inclined to the W ( $\text{PA} \approx -20^\circ$ ).

Based on these findings, we consider the alternative possibility that the velocity gradient is tracing a disk. To analyze the kinematics of the gas in more detail, we fitted the  $\text{CH}_3\text{CN}$  emission in each  $0.4 \text{ km s}^{-1}$  velocity channel with a 2D Gaussian. This allowed us to derive the peaks of the line emission at different velocities. Then all peaks can be plotted together to obtain a picture of the gas velocity field. This is done in Fig. 4a, where for each peak we also plot the corresponding 50% contour level to give an idea of the size of the gas emitting at that velocity.

Two considerations are in order. The first is that the peaks outline a sort of elliptical pattern, roughly centered on the position of the continuum peak and oriented SSE–NNW. The second is that the most blue- and red-shifted peaks tend to converge towards the position of the sub-mm continuum peak. On this basis, one is tempted to hypothesize that the  $\text{CH}_3\text{CN}$  emission is tracing Keplerian-like rotation, since this would explain why the emission both at systemic velocities and at high (blue- and red-shifted) velocities are observed towards the rotation center.

With this in mind, we fitted the observed velocity pattern assuming Keplerian rotation about a point-like source. We stress that ours is a purely kinematical fit, where only the rotation velocity in a 2D disk is calculated, and no estimate of the observed line intensity was computed. Also, no attempt was made to demonstrate the uniqueness of the model proposed, and we envisage the possibility that other interpretations might be possible. Our simple model is sufficient to constrain a number of important parameters. The inputs of the model are the LSR velocity of the system ( $V_{\text{sys}}$ ), the central point mass ( $M_*$ ) and its position ( $x_0, y_0$ ), the inclination angle ( $\theta$ ) of the rotation axis with respect to the plane of the sky, and the position angle ( $\psi$ ) of the projected major axis of the disk.

The best fit was obtained by varying all input parameters inside reasonable ranges and minimizing the expression  $\sum_i (V_i^{\text{observed}} - V_i^{\text{model}})^2$  where  $i$  indicates the peak in a generic velocity channel. For our calculations, we used the  $K = 2, 3$ , and 4 components of the  $\text{CH}_3\text{CN}(19-18)$  transition, as well as other prominent lines of other species, such as  $\text{CH}_3\text{OH}(7_{1,6}-6_{1,5}) v_t = 1$ ,  $\text{CH}_3\text{OH}(14_{1,13}-14_{0,14})$ , and  $\text{HC}_3\text{N}(37-36)$ . All of these lines reveal a kinematical pattern very similar to the one in Fig. 4a, demonstrating that such a pattern does not depend on the tracer and mirrors a real physical structure. In Fig. 4b we show an overlay of the velocity peaks of all the lines and a velocity map of the best-fit model. Clearly, the agreement between the computed and observed LSR velocities is remarkable. The best-fit parameters are the following:  $V_{\text{sys}} = 30.0 \pm 0.3 \text{ km s}^{-1}$ ,

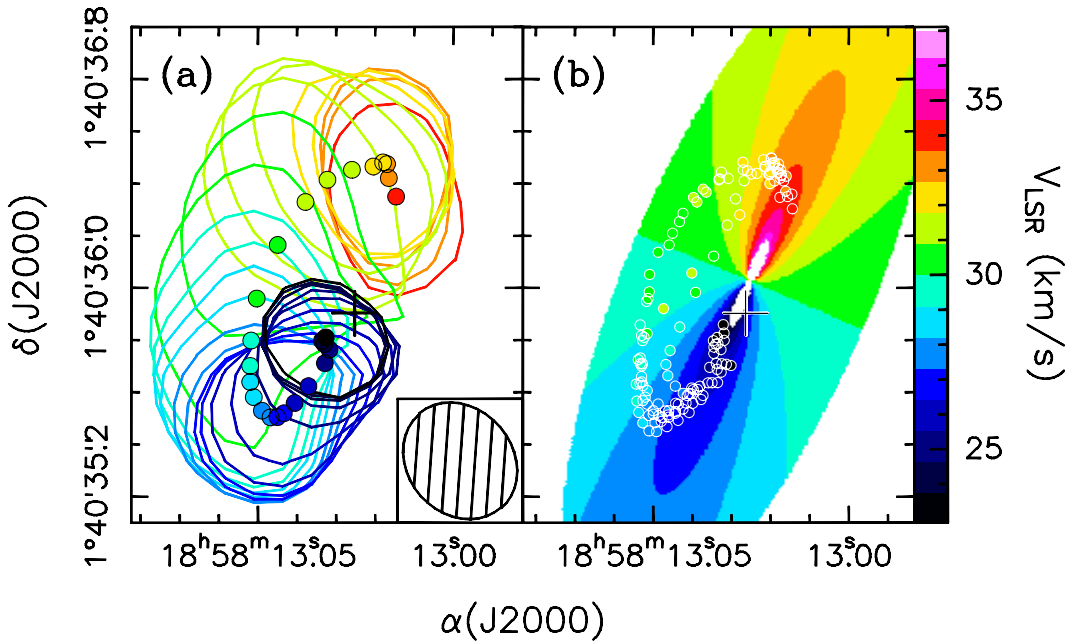


**Fig. 4.** a) Peaks of the  $\text{CH}_3\text{CN}(19-18)$   $K = 2$  line emission (solid circles) obtained with a 2D Gaussian fit channel by channel. For each peak the corresponding 50% contour level is also drawn (using the same color as the peak). The color corresponds to the line-of-sight velocity, according to the scale displayed to the right. The ellipse in the bottom right denotes the synthesized beam. b) Comparison between the velocity of the best-fit Keplerian disk (color map) and the emission peaks at different velocities (solid circles) obtained for the following lines:  $\text{CH}_3\text{CN}(19-18)$   $K = 2, 3, 4$ ,  $\text{CH}_3\text{OH}(7_{1,6}-6_{1,5})$   $v_t = 1$ ,  $\text{CH}_3\text{OH}(14_{1,13}-14_{0,14})$ , and  $\text{HC}_3\text{N}(37-36)$ . The crosses mark the position of the continuum peak.

$x_0 = 18^{\text{h}}58^{\text{m}}13^{\text{s}}027 \pm 0^{\text{.}}002$ ,  $y_0 = 01^{\circ}40'35''.94 \pm 0^{\text{'}}07$ ,  $\psi = 157 \pm 4^\circ$ ,  $\theta = 19 \pm 1^\circ$ , and  $M_* = 18 \pm 3 M_\odot$ .

A lower limit for the disk radius is  $R_{\text{disk}} \approx 2500$  AU, obtained from the maximum deprojected distance of the peaks from the center. One may wonder if such a big structure can undergo Keplerian rotation. The mass of the disk can be estimated from the continuum emission. The integrated flux density from core B at 350 GHz is 0.32 Jy. Assuming a dust absorption coefficient  $0.5 \text{ cm}^2 \text{ g}^{-1}$  ( $\nu/230.6 \text{ GHz}$ ) (Kramer et al. 2003) and a gas-to-dust mass ratio of 100, we obtain  $\sim 3 M_\odot$  for a dust temperature of 100 K. Despite the large uncertainties on the dust opacity and temperature, we believe that the mass of core B is significantly less than the central mass ( $\sim 18 M_\odot$ ), which satisfies the condition for Keplerian rotation.

It is worth stressing that our findings are in good agreement with the recent study by Ilee et al. (2012). Through measurements of scattered light from G35.20-0.74N, these authors find that the CO first overtone bandhead emission at  $2.3 \mu\text{m}$  can be fitted with a Keplerian disk rotating about a  $17.7 M_\odot$  star.

The distribution of the molecular peaks in Fig. 4b clearly shows that our observations detect only the NE side of the disk. We speculate that this could be an opacity effect. If the disk is optically thick in the relevant lines, flared, and inclined by  $19^\circ$ , only part of the surface heated by the star is visible to the observer. This creates an asymmetry along the direction of the projected disk axis, with line emission being more prominent on the side (in our case the NE side) where the disk surface is visible. Clearly, radiative transfer calculations are needed to confirm this scenario, but we note that in our source the NE part of the disk axis should be pointing towards the observer, consistent with the orientation of the CO outflow (blue-shifted to the NE and red-shifted to the SW – see GHLW) and the obscuration seen to the SW in the IR images (see Fig. 2).

#### 4. The stellar content of core B: A binary system?

An issue that is worth discussing is whether an  $18 M_\odot$  YSO is compatible with the bolometric luminosity of the region. ( $3 \times 10^4 L_\odot$ ; see Sect. 1). Depending on the adopted mass–luminosity relation, the luminosity expected for an  $18 M_\odot$  star

ranges from  $2.5 \times 10^4 L_\odot$  (Diaz-Miller et al. 1998), to  $6.6 \times 10^4 L_\odot$  (Martins et al. 2005). This means that the  $18 M_\odot$  star should be the main contributor to the luminosity of the whole star forming region. Such a possibility seems quite unlikely due to the presence of multiple cores (see Fig. 2), one of which is an HMC possibly hosting at least another high-mass star (core A).

A possibility is that one is underestimating the true luminosity due to the “flashlight effect”, where part of the stellar photons are lost through the outflow cavities. According to the recent model by Zhang et al. (2013), when this effect is taken into account, the luminosity obtained assuming isotropic emission ( $3.3 \times 10^4 L_\odot$ ) becomes as high as  $7 \times 10^4 - 2.2 \times 10^5 L_\odot$ , consistent with a single star of  $\sim 20-34 M_\odot$ .

While the previous explanation is possible, the isotropic estimate appears more robust than a model-dependent value, and we thus consider another hypothesis, namely that one is dealing with a binary system. In this case, the luminosity is significantly reduced with respect to that of a single  $18 M_\odot$  object and may be as low as  $\sim 7 \times 10^3 L_\odot$  for equal members. The latter is much less than the bolometric luminosity, thus allowing for a significant contribution by other YSOs.

The existence of a binary system could also explain why the N–S jet associated with core B is not aligned with the disk rotation axis. The presence of a companion would in fact be sufficient to induce precession of the jet/outflow, as hypothesized by Shepherd et al. (2000) to explain the observed precession of the bipolar outflow from the high-mass protostar IRAS 20126+4104. In this scenario, the outflow from core B would precess about an axis oriented NE–SW, i.e. along the bisector of the butterfly-shaped IR nebula seen in Fig. 1. The IR emission would arise from the cavity opened by the outflow itself during its precession, while the thermal radio jet would trace the current direction of the precessing axis.

The last question we address is the origin of the free-free emission from core B (see e.g. Fig. 3). Could this be tracing a (hypercompact) HII region? According to GHLW, this source (N. 7 in their Table 1) has a spectral index  $>1.3$  between 6 and 3.6 cm, compatible with free-free emission from an optically thick HII region. Extrapolation of the 3.6 cm flux density (0.5 mJy) to 1.3 cm gives  $>1.9$  mJy, in agreement with

the 3 mJy flux measured, with lower angular resolution, by Codella et al. (2010). It is thus possible that the emission is partially thick at 1.3 cm, and the Lyman continuum estimate of  $10^{45} \text{ s}^{-1}$  obtained under the optically thin assumption is a lower limit. A binary system with a total mass of  $18 M_{\odot}$  has a Lyman continuum flux (see Diaz-Miller et al. 1998) ranging from  $5 \times 10^{44} \text{ s}^{-1}$  (for equal masses) to  $1.8 \times 10^{47} \text{ s}^{-1}$ . We conclude that we could be observing an HII region ionized by a binary system at the center of a Keplerian disk. Should this be confirmed, G35.20–0.74N would represent a unique example of radio jet coexisting with an HII region powered by the same YSO(s). Investigating such a short-lived transition phase in the evolution of an OB-type star could provide us with important clues to the formation process of these objects.

*Acknowledgements.* It is a pleasure to thank Göran Sandell for stimulating discussions of the G35.20–0.74N region and the anonymous referee for constructive criticisms. We also acknowledge the support of the European ALMA Regional Center and the Italian ARC node. This paper makes use of the following ALMA data: ADS/JAO.ALMA#2011.0.00275.S. ALMA is a partnership of ESO (representing its member states), NSF (USA), and NINS (Japan), together with NRC (Canada) and NSC and ASIAA (Taiwan), in cooperation with the Republic of Chile. The Joint ALMA Observatory is operated by ESO, AUI/NRAO, and NAOJ. This work also used observations made with the *Spitzer* Space Telescope, which is operated by the Jet Propulsion Laboratory, California Institute of Technology, under a contract with NASA. MSNK is supported by a Ciência 2007 contract, funded by FCT (Portugal) and POPH/FSE (EC).

## References

- Benjamin, R. A., Churchwell, E., Babler, B. L., et al. 2003, *PASP*, 115, 953  
 Birks, J. R., Fuller, G. A., & Gibb, A. G. 2006, *A&A*, 458, 181 (BFG)  
 Bonnell, I. A., & Bate, M. R. 2006, *MNRAS*, 370, 488  
 Brebner, G. C., Heaton, B., Cohen, R. J., & Davies, S. R. 1987, *MNRAS*, 229, 679  
 Cesaroni, R., Galli, D., Lodato, G., Walmsley, C. M., & Zhang, Q. 2007, in *Protostars and Planets V*, eds. B. Reipurth, D. Jewitt, & K. Keil (Tucson: Univ. of Arizona Press), 197  
 Codella, C., Cesaroni, R., López-Sepulcre, A., et al. 2010, *A&A*, 510, A86  
 De Buizer, J. M. 2006, *ApJ*, 642, L57  
 Dent, W. R. F., Little, L. T., Kaifu, N., Ohishi, M., & Suzuki, S. 1985, *A&A*, 146, 375  
 Dent, W. R. F., Little, L. T., Sato, S., Ohishi, M., & Yamashita, T. 1985, *MNRAS*, 217, 217  
 Diaz-Miller, R. I., Franco, J., & Shore, S. N. 1998, *ApJ*, 501, 192  
 Dutrey, A., Guilloteau, S., & Ho, P. 2007, in *Protostars and Planets V*, eds. B. Reipurth, D. Jewitt, & K. Keil (Tucson: Univ. of Arizona Press), 495  
 Estalella, R., Mauersberger, R., Torrelles, J. M., et al. 1993, *ApJ*, 419, 698  
 Fuller, G. A., Zijlstra, A. A., & Williams, S. J. 2001, *ApJ*, 555, L125  
 Gibb, A. G., Hoare, M. G., Little, L. T., & Wright, M. C. H. 2003, *MNRAS*, 339, 1011 (GHLW)  
 Heaton, B. D., & Little, L. T. 1988, *A&A*, 195, 193  
 Ilee, J. D., Wheelwright, H. E., Oudmajer, R. D., et al. 2013, *MNRAS*, 429, 2960  
 Keto, E. 2007, *ApJ*, 666, 976  
 Kramer, C., Richer, J., Mookerjee, B., Alves, J., & Lada, C. 2003, *A&A*, 399, 1073  
 Krumholz, M. R., Klein, R. I., McKee, C. F., Offner, S. S. R., & Cunningham, A. J. 2009, *Science*, 323, 754  
 Lee, H.-T., Takami, M., Duan, H.-Y., et al. 2012, *ApJS*, 200, 2  
 Little, L. T., Dent, W. R. F., Heaton, B., Davies, S. R., & White, G. J. 1985, *MNRAS*, 217, 227  
 Little, L. T., Kelly, M. L., & Murphy, B. T. 1998, *MNRAS*, 294, 105  
 López-Sepulcre, A., Codella, C., Cesaroni, R., Marcelino, N., & Walmsley, C. M. 2009, *A&A*, 499, 811  
 Martins, F., Schaerer, D., & Hillier, D. J. 2005, *A&A*, 436, 1049  
 Shepherd, D. S., Yu, K. C., Bally, J., & Testi, L. 2000, *ApJ*, 535, 833  
 Velusamy, T., Marsh, K. A., Beichman, C. A., Backus, C. R., & Thompson, T. J. 2008, *AJ*, 136, 197  
 Walther, D. M., Aspin, C., & McLean, I. S. 1990, *ApJ*, 356, 544  
 Wang, K.-S., van der Tak, F. F. S., & Hogerheijde, M. R. 2012, *A&A*, 543, A22  
 Zhang, Q., Hunter, T. R., Beuther, H., et al. 2007, *ApJ*, 658, 1152  
 Zhang, B., Zheng, X. W., Reid, M. J., et al. 2009, *ApJ*, 693, 419  
 Zhang, Y., Tan, J. C., De Buizer, J. M., et al. 2013, *ApJ*, in press [[arXiv:1302.38582](https://arxiv.org/abs/1302.38582)]  
 Zinnecker, H., & Yorke, H. W. 2007, *ARA&A*, 45, 481